Hindawi Publishing Corporation
Journal of Nanotechnology
Volume 2012, Article ID 794874, 9 pages
doi:10.1155/2012/794874

Research Article

Photocatalytic Oxidation of Carbon Monoxide over NiO/SnO_2 Nanocomposites under UV Irradiation

R. M. Mohamed[1,2] and Elham S. Aazam[1]

[1] *Chemistry Department, Faculty of Science, King Abdulaziz University, P. O. Box 80203, Jeddah 21589, Saudi Arabia*
[2] *Nanostructured Material Division, Advanced Materials Department, Central Metallurgical R&D Institute, Helwan 11421, Cairo, Egypt*

Correspondence should be addressed to R. M. Mohamed, redama123@yahoo.com

Received 18 May 2011; Accepted 19 June 2011

Academic Editor: Yuanhui Zheng

The NiO/SnO_2 nanocomposites have been prepared by the simple coprecipitation method and further characterized by the XRD, SEM, TEM, UV-Vis, and BET. X-ray diffraction (XRD) data analyses indicate the exclusive formation of nanosized particles with rutile-type phase (tetragonal SnO_2) for Ni contents below 10 mol%. Only above 10 mol% Ni, the formation of a second NiO-related phase has been determined. The particle size is in the range from 12 to 6 nm. It decreases with increasing amounts of doping NiO. The morphology of NiO-doped SnO_2 nanocrystalline powders is spherical, and the distribution of particle size is uniform, as seen from transmission electron microscopy (TEM). The photocatalytic oxidation of CO over NiO/SnO_2 photocatalyst has been investigated under UV irradiation. Effects of NiO loading on SnO_2, photocatalyst loading, and reaction time on photocatalytic oxidation of CO have been systematically studied. Compared with pure SnO_2, the 33.3 mol% NiO/SnO_2 composite exhibited approximately twentyfold enhancement of photocatalytic oxidation of CO. Our results provide a method for pollutants removal. Due to simple preparation, high photocatalytic oxidation of CO, and low cost, the NiO/SnO_2 photocatalyst will find wide application in the coming future of photocatalytic oxidation of CO.

1. Introduction

The wide variety of electronic and chemical properties of metal oxides makes them exciting materials for basic research and technological applications alike. Metal oxides span a wide range of electrical and optical properties from wide band gap insulators and lasers to metallic, superconducting, and field-emitting materials. Enormous efforts are being directed towards the development of nanometer-sized metal oxides in studies related to their fundamental mechanisms such as size effect and quantum effect and towards the applications of these materials. Particle sizes in the nanoregime and specific crystal morphologies are expected to enhance the performance and allow the fine tuning of the properties of these materials. The optical properties of semiconducting nanoparticles have recently been a subject of great interest. Tin oxide (SnO_2) is a versatile wide band gap (3.6 eV at 300 K) n-type semiconducting oxide with a wide variety of applications.

Semiconductors with wider band gaps exhibit better stability than those with small and medium band gaps, but show lower light-harvesting ability in visible light [1]. Therefore, coupling of semiconductors with different band gaps is good approach to prepare photocatalysts with high activity and good stability. The excited electrons can transfer in coupled semiconductors from the high conduction band to the low one, leading to efficient separation of photogenerated electron-hole pairs.

Enhancements in photocatalytic activity over coupled semiconductors including CdS/TiO_2 [2], ZnS/TiO_2 [3], Cu_2O/TiO_2 [4], and CuO/TiO_2 [5, 6], $WO_3/SiCeTiO_2$ [7], $SrTiO_3/TiO_2$ [8], SnO_2/TiO_2 [9], Ta_2O_5/TiO_2 [10], $CuO/Al_2O_3/TiO_2$ [11] have been investigated extensively.

The SnO_2 exhibits good activity and stability under irradiation in both acidic and basic media. However, the pure SnO_2 shows much lower photocatalytic activity even under UV irradiation due to its large band gap (3.8 eV) [1].

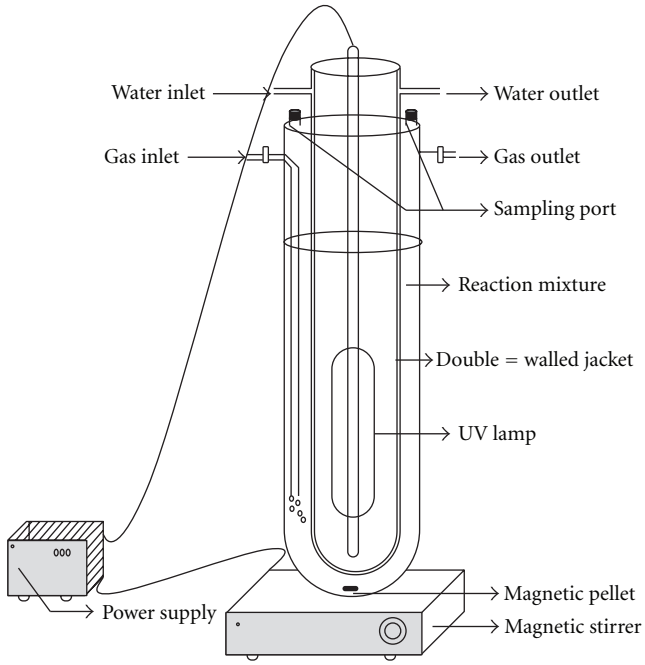

Figure 1: Schematic representation of photoreactor.

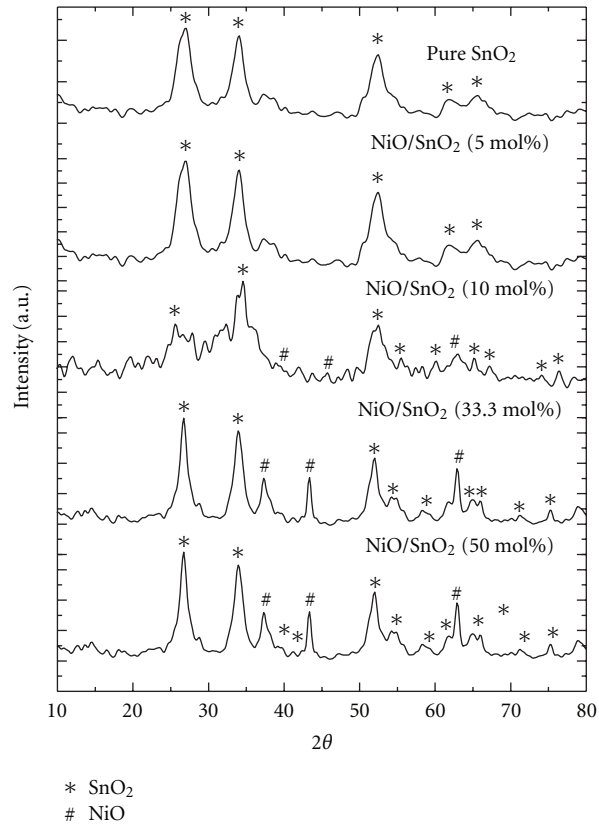

Figure 2: XRD patterns of pure and nickel-doped SnO_2 nanoparticles.

To improve its photocatalytic activity, it is necessary to couple SnO_2 with another semiconductor with lower band gap. The NiO is a p-type semiconductor with a small band gap. If the SnO_2 is coupled with the NiO, the n-SnO_2/p-NiO heterojunctions can be formed in the interface. The photogenerated electrons from SnO_2 can easily migrate to NiO. This favors the separation of photogenerated electrons with holes, leading to enhancement of photocatalytic activity. The CuO/SnO_2 nanocomposites have been studied as gas sensor materials [12–14] or electrochemical materials [15].

To our knowledge, there is a little information regarding photocatalytic oxidation of CO using NiO/SnO_2 nanocomposite. This prompts us to synthesize and to investigate the photocatalytic performance of NiO/SnO_2 nanocomposite. The objective of this study is to a highly efficient, cost-effective NiO/SnO_2 photocatalyst. The NiO/SnO_2 photocatalysts have been prepared by simple coprecipitation method and characterized by XRD, SEM, UV-vis, TEM, and BET. Effects of different variables on photocatalytic oxidation of CO have been investigated in detail, including NiO content, photocatalyst loading, and reaction time.

2. Experimental Method

2.1. Preparation of NiO/SnO_2 Nanocomposite. The NiO/SnO_2 composites have been prepared by the simple coprecipitation method. $SnCl_4 \cdot 5H_2O$ and $NiSO_4 \cdot 5H_2O$ are used as starting materials. Typically, $SnCl_4$ and $NiSO_4$ with a desired molar ratio are mixed together in distilled water. The obtained solution is continuously stirred at 80°C; meanwhile, the NaOH solution is added with at a rate of 0.02 mL/s until complete precipitation (solution pH value above 11). After continuous stirring for another 2 h, the precipitate is filtered and washed thoroughly with distilled water until free of Cl ion and SO_4 ion. Finally, the precipitate is dried at 100°C for 24 h and calcined at 550°C for 5 h to obtain NiO/SnO_2 nanocomposite. The NiO content in final composite is calculated by the concentration of $NiSO_4$ solution used during preparation. The NiO/SnO_2 is denoted by the molar percentage of NiO in photocatalyst (mol% = n_{NiO}/n_{SnO_2}).

2.2. Characterization. The structure of the catalyst was examined by X-ray diffraction (XRD) on a Rigaku X-ray diffractometer system equipped with as RINT 2000 wide angle Joniometer using Cu Kα radiation and a power of 40 kV × 30 mA. The intensity data were collected at 25°C over a 2θ range of 10–80°. The UV-vis diffuse reflectance absorption spectra were recorded with a Shimadzu UV-2450 at 295 K. N_2-adsorption measurement was carried out at 77 K using Nova 2000 series, Chromatech. Prior to analysis, the samples were outgassed at 250°C for 4 h. The morphology and particle size of the prepared samples were examined via a transmission electron microscope (Hitachi H-9500 operated at 300 kv).

2.3. Photocatalytic Activity Tests. In this section, we used quartz photoreactor as shown in Figure 1. UV irradiation was performed by a 150 W medium pressure xenon lamp

Table 1: Variation of particle size, lattice parameter and band gap with dopant concentration.

Dopant concentration (%)	Crystallite size (nm)	Lattice parameter a (Å)	Lattice parameter c (Å)	Band gap (eV)
0.0	5.0	4.800	3.197	3.63
5.0	3.8	4.793	3.192	3.49
10.0	3.0	4.792	3.187	3.40
33.3	2.7	4.786	3.185	3.29
50.0	2.0	4.784	3.183	3.21

Table 2: Texture parameters of pure and nickel-doped SnO_2 nanoparticles.

Catalyst systems	S_{BET} (m^2/g)	S_t (m^2/g)	Total V_P (mL/g)	r (Å)	C_{BET}
Pure SnO_2	30.00	26.00	0.030	28.00	9.00
NiO/SnO_2 (5 mol%)	34.00	48.00	0.100	65.00	20.00
NiO/SnO_2 (10 mol%)	40.00	44.00	0.160	91.00	58.00
NiO/SnO_2 (33.3 mol%)	45.00	56.00	0.034	18.00	52.00
NiO/SnO_2 (50 mol%)	42.00	40.00	0.073	31.00	63.00

S_{BET}: BET surface area.
S_t: surface area derived from V_{l-t} plots.
r: mean pore radius.
V_p: total pore volume.

placed inside a quartz jacket and equipped with a cooling tube. Photooxidation reactions were carried out suspending 0.2 g of the prepared catalyst. A feed gas of ca. 400 ppmV CO was made up of CO (purity 99.99%) and air and was stored in a high-pressure cylinder. Samples were withdrawn at regular intervals from the upper part of the reactor. The Photooxidation rate was determined by measuring the CO consumed using a gas chromatograph Shimadzu GCMS-QP 5050A and a gas-sampling valve. The removal efficiency of CO has been calculated by applying

$$\%\text{Removal efficiency} = \frac{C_0 - C}{C_0 \times 100}, \quad (1)$$

where C_0 the original CO content, C the retained CO.

3. Results and Discussions

3.1. Characterization of NiO/SnO_2 Photocatalyst

3.1.1. XRD Analyses. The typical XRD patterns of the pure and Ni-doped SnO_2 samples annealed at 550°C are shown in Figure 2. The peak positions of each sample exhibit the rutile type tetragonal structure of SnO_2 which were confirmed from the ICDD card no. 77-0452. Further, no other impurity peak was observed in the XRD pattern showing the single phase sample formation. The crystalline size of all the samples was calculated using Scherer formula [16], $D = 0.9\lambda/\beta \cos\theta$, where λ is the wavelength of X-ray radiation, β is the full width at half maximum (FWHM) of the peaks at the diffracting angle θ. The calculated particle sizes of each sample are given in Table 1. It can be observed from Table 1 that the crystalline size of SnO_2 decreased from 5 nm to 2 nm when Ni^{2+} content increased from 0% to 50%. The data revealed that the presence of Ni^{2+} ions in SnO_2 prevented the growth of crystal grains. The variations in the lattice parameter have also been studied for different doping concentrations and presented in Figure 3. The ionic radius of Ni^{2+} is 69 pm, whereas that of Sn^{4+} is 71 pm. The Ni ions substitute the Sn^{4+} ions in the crystal due to comparable ionic radius. However, the decrease in the lattice parameter may be due to the smaller ionic radius of Ni ions.

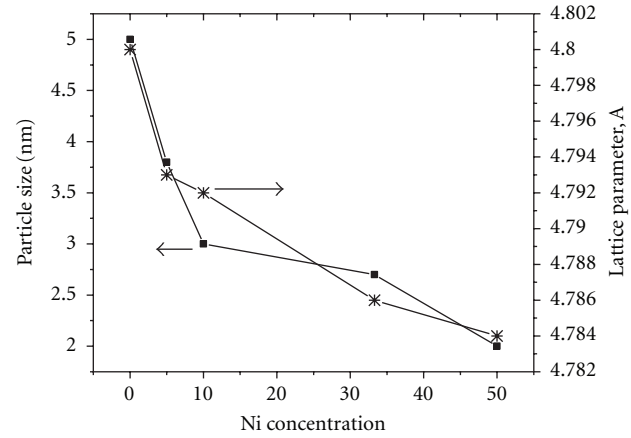

Figure 3: Variation of particle size and lattice parameter with nickel concentration.

3.1.2. Specific Surface Area Trends. The surface parameters of surface area and the data calculated from the t-plot were estimated by the low-temperature nitrogen adsorption at relative pressures (P/P^0) in the range of 0.05–0.9 and are given in Table 2. The N_2 adsorption isotherms for pure and nickel-doped SnO_2 nanoparticles (Figure 4) are typical of type II. Specific surface area measurements of SnO_2-based powders show that nickel additives drastically influence the morphology of the powders. Table 2 summarizes S_{BET} data and is an evidence that the addition of Ni increases the surface area, because The addition of NiO prevents the

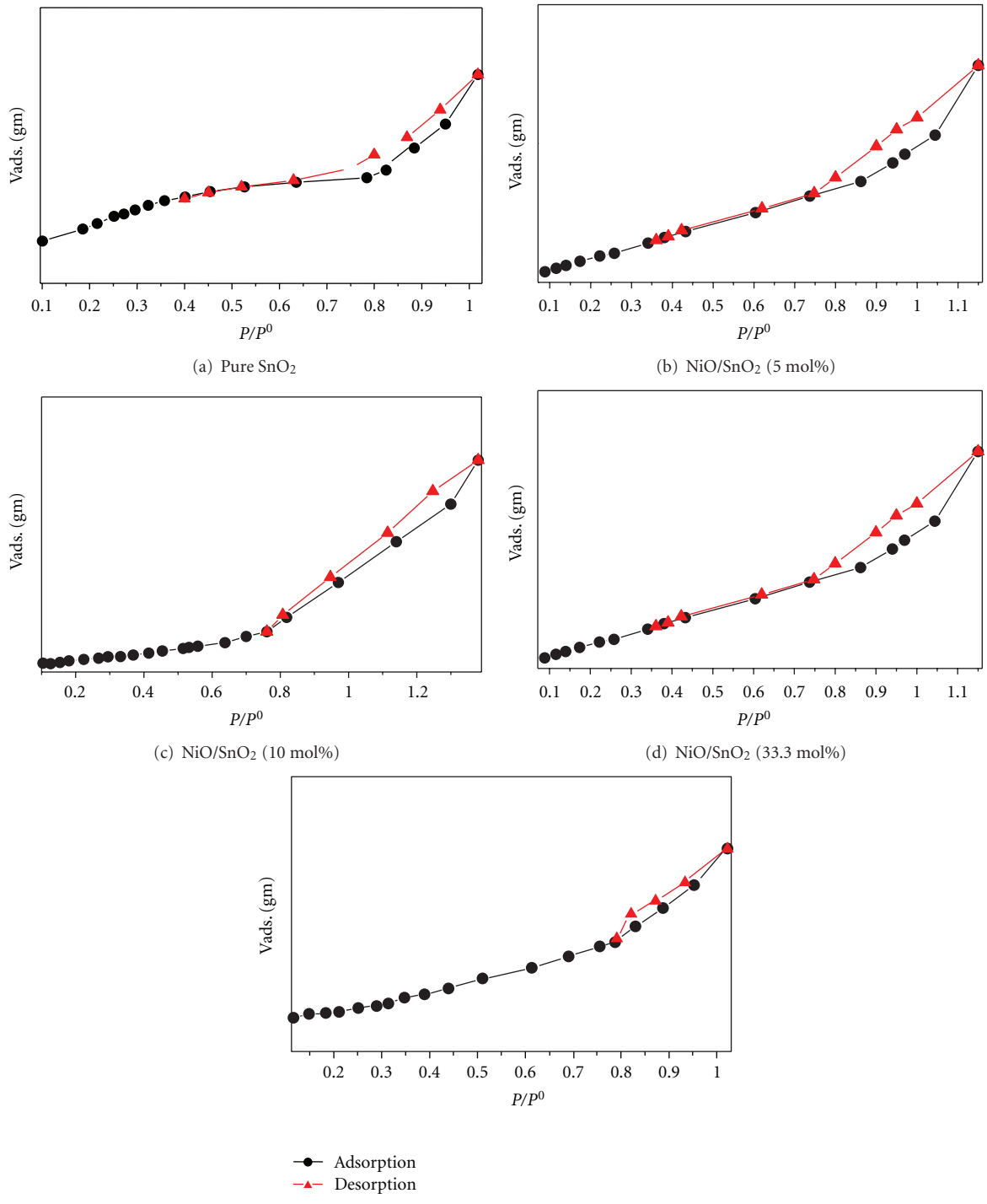

FIGURE 4: N_2 sorption isotherms of pure and nickel-doped SnO_2 nanoparticles.

densification and growth of SnO_2 grain and consequently results in more porous micro structure than pure SnO_2 [17].

3.1.3. Optical Properties. Absorption is powerful nondestructive technique to explore the optical properties of semiconducting nanoparticles. The optical absorption spectra of pure and Ni doped SnO_2 nanoparticles are shown in Figure 5. The absorption edge of different samples varies, as the concentration of Ni in the SnO_2 nanoparticles varies. In order to calculate the direct band gap we used the Tauc relation

$$\alpha h\nu = A\left(h\nu - E_g\right)^{1/2}, \tag{2}$$

where α is the absorption coefficient, A is a constant. $n = 1/2$ for direct band gap semiconductor. An extrapolation of the

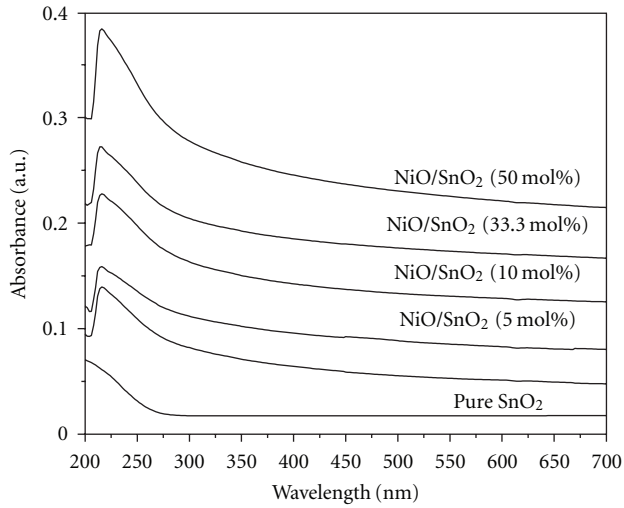

Figure 5: UV-V is absorption spectrum of pure and nickel-doped SnO_2 nanoparticles.

linear region of a plot of $(\alpha h\nu)^2$ versus $h\nu$ gives the value of the optical band gap E_g (Table 1). The measured band gap was found to be 3.63 eV for undoped SnO_2 nanoparticles, which is similar to the reported value of the bulk SnO_2, that is, 3.6 eV [18]. This can be attributed to the quantum confinement effect of the nanoparticles [19]. On doping with nickel, the band gap energy decreases (Table 1) even though the particle size decreases. This is in contrast to the normal phenomenon of quantum confinement. Chun-Ming et al. have already reported band gap narrowing effect for doped SnO_2 nanoparticles [20]. However, there is no clear understanding of this phenomenon. A direct-indirect transition have been proposed by Rakhshani et al. [21] In order to explain the band gap narrowing effect, many groups have suggested that alloying effect of parent compound with some impurity phases may be responsible for the band gap narrowing [20, 22, 23]. In one hand, the alloying effect from SnO_2-NiO can be neglected, because the band gap decreases below the band gap energy of NiO (3.54 eV) [24]. The samples containing up to 10% Ni concentration, SnO_2-SnO_2-x alloying effect may be responsible for the band gap narrowing effect. For the SnO_2 nanoparticles above 10% Ni concentration, there is a huge drop in the band gap. This may be due to the formation of subbands in between the band gap, and the conduction band and subbands are merging with the conduction band to form a continuous band.

3.1.4. SEM and TEM. Figure 6 shows the typical morphology and composition of pure and Ni-doped SnO_2 nanoparticles. Figure 6 shows the presence of large spherical aggregates of smaller individual nanoparticles and the presence of Ni is confirmed from the selective area EDAX analysis (Table 3). It can be verified from the results of XRD and EDAX that the Ni is successfully doped in the SnO_2 nanocrystals.

Figures 7(a) and 7(b) show TEM images taken for pure and 33.3% Ni-doped SnO_2 nanoparticles, respectively. Powder samples were dispersed in ethanol and sonicated in an ultrasonic bath for fifteen minutes for TEM analysis. It is observed from Figure 7 that SnO_2 grains have a spherical morphology with an average diameter of 12 nm for pure SnO_2 and 6 nm for 5% Ni-doped SnO_2, confirming the reduction in particle size as a result of Ni doping in SnO_2. Particle size obtained from TEM analysis is slightly higher than the crystallite size calculated from XRD spectra.

3.2. Photocatalytic Activity

3.2.1. Effect of NiO Content on Photocatalytic Oxidation of CO. An increase in the lifetime of photogenerated electron-hole pairs in coupled oxides, due to electrons transfer between the two coupling oxides, seems to be critical to the enhancement for photocatalytic oxidation of CO. In consequence, the NiO content in NiO/SnO_2 nanoparticles plays an important role for photocatalytic oxidation of CO. Figure 8 shows effect of NiO content in composites on photocatalytic oxidation of CO. As illustrated in Figure 8, the pure SnO_2 exhibited very poor activity for photocatalytic oxidation of CO. With the increment of NiO amount from 0.0 to 10 mol%, the photocatalytic oxidation of CO increases sharply. It increases slightly when NiO content is varied from 10 to 33.3 mol%. However, further increment of NiO to 50 mol% leads to a progressive decrease in photocatalytic oxidation of CO. The optimum NiO content in NiO/SnO_2 composites is about 33.3 mol%. Compared with pure SnO_2, the 33.3 mol% NiO/SnO_2 composite exhibits approximately twentyfold enhancement of photocatalytic oxidation of CO. NiO or SnO_2 alone shows poor photocatalytic activity for photocatalytic oxidation of CO, suggesting that the coexistence is responsible for the enhancement of photocatalytic activity. Since the conduction band of NiO is lower than that of SnO_2, excited electrons from SnO_2 can easily transfer to NiO. Accumulation of excess electrons leads to a negative shift in the Fermil level of NiO [25, 26]. Thus, the NiO on the SnO_2 acts as active sites, where the photocatalytic reactions take place. The efficient interface electrons transfer inhibits the quick recombination of the photogenerated electron-hole pairs on SnO_2 surface, leading to enhancement of photocatalytic activity of NiO/SnO_2 composites. There exists an optimal amount when noble metals or metal oxides are loaded on TiO_2 surface [26–28]. Similar dependence has been observed when the NiO is loaded on the SnO_2 surface. When NiO content is below optimal level, the number of active trapping sites at NiO/SnO_2 interface is enhanced with the increment of NiO amount, consequently resulting in an increase in photocatalytic oxidation of CO. However, when NiO content is above optimal level, the light sensitization of SnO_2 is blocked by the excess surrounding NiO, resulting in a lower density of the excited electrons accumulation on NiO [26]. As a result, the photocatalytic oxidation of CO is lowered due to inefficient excitation.

3.2.2. Effect of Photocatalyst Concentration. Apart from NiO content, the photocatalyst concentration is also an important factor for the photocatalytic oxidation of CO. To quantify

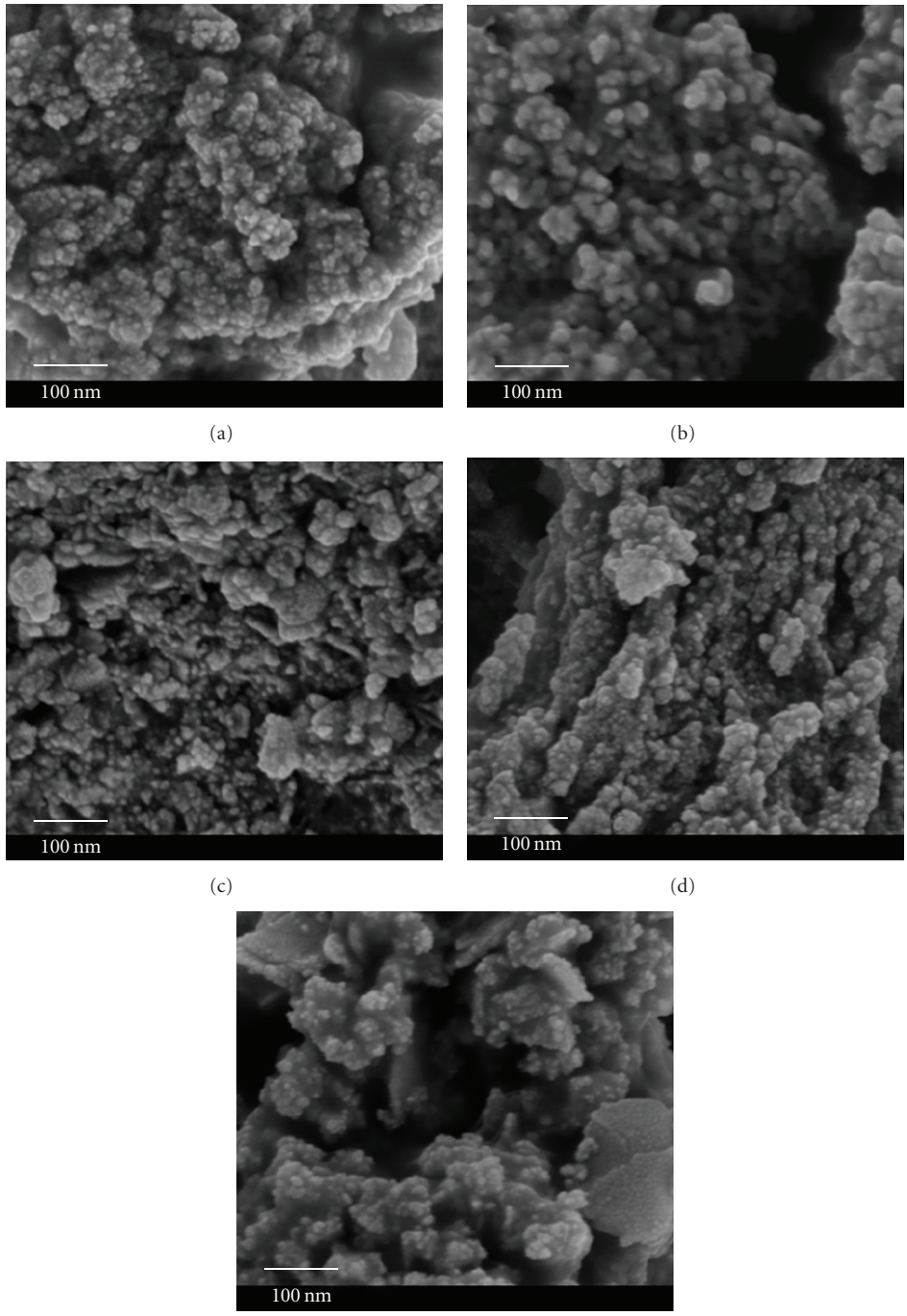

Figure 6: SEM images of the typical morphology and composition of pure (a), 5, 10, 33.3, and 50 % Ni doped ((b), (c), (d), and (f), resp.) SnO_2 nanoparticles.

Table 3: NiO/SnO_2 atomic % ratio of the produced samples measured by EDX Technique at three areas.

NiO/SnO_2 molar ratio	NiO/SnO_2 atomic % ratio			Average NiO/SnO_2 atomic % ratio
	*A*1	*A*2	*A*3	
0.0	0.00	0.00	0.00	0.00
5.0	5.00	4.99	5.00	4.99
10.0	10.0	9.98	9.99	9.99
33.3	33.30	33.3	33.30	33.30
50.0	50.00	50.05	50.02	50.02

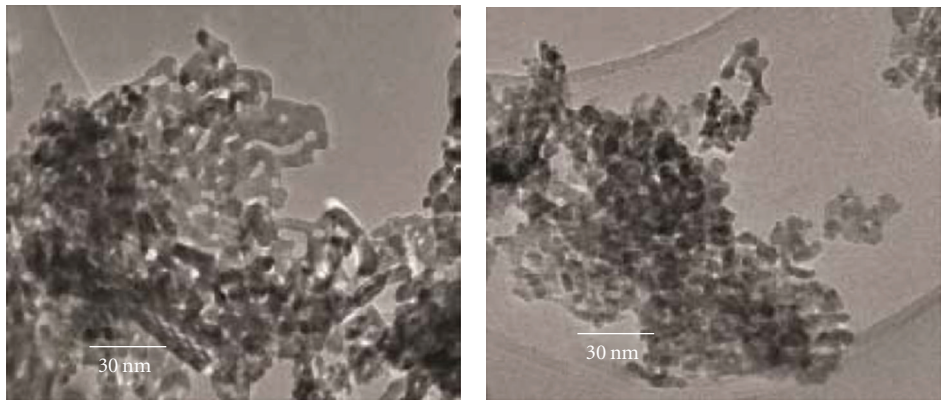

(a) (b)

Figure 7: TEM images of (a) pure and (b) 33.3 mol% nickel-doped SnO_2 nanoparticles.

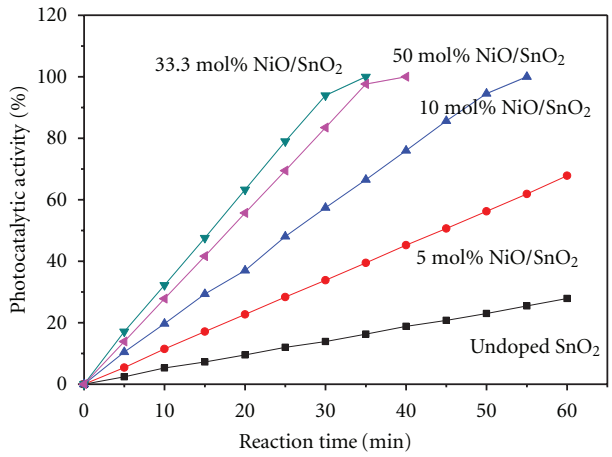

Figure 8: Photooxidation of CO over pure and nickel-doped SnO_2 nanoparticles.

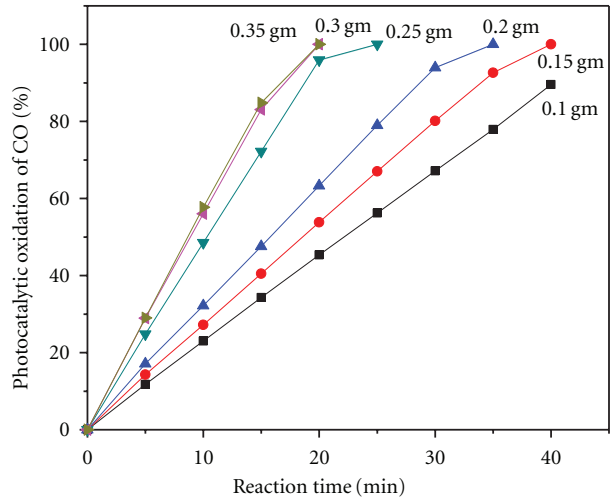

Figure 9: Photooxidation of CO over different loading from 33.3 mol% NiO/SnO_2 calcined at 550°C Figure 10. Kinetic for photooxidation of CO over loading from 33.3 mol% NiO/SnO_2 calcined at 550°C.

the dependence of CO oxidation on photocatalyst concentration, the photocatalytic oxidation of CO at various catalyst concentrations have been investigated (Figure 9). As shown in Figure 9, with the increment of photocatalyst concentration from 0.1 to 0.2 g, the photocatalytic CO oxidation is gradually increased. However, it is progressively decreased when photocatalyst concentration is changed from 0.2 to 0.35 g. A similar dependence has been reported with the use of Pt/TiO_2 as photocatalyst, which is typical for reaction occurring in suspension [29, 30]. The photocatalytic reactions in suspension are determined by trapping sites on photocatalyst surface and by the light transmission in suspension. At a low photocatalyst concentration, the rate of photocatalytic reactions is mainly limited by the number of trapping sites which is increased with the increment of photocatalyst concentration. However, when photocatalyst concentration is above optimal level, the suspension becomes turbid. The light is unable to penetrate the suspension due to scattering by the suspended photocatalyst particles, leading to a sharp decrement in photocatalytic CO oxidation.

The reaction order with respect to CO was determined by plotting reaction time versus log[CO] according to the following equation for various 33.3 mol% NiO/SnO_2 loading:

$$\mathrm{Log}[C]_t = -kt + \mathrm{Log}[C]_o, \tag{3}$$

where $[C]_t$ and $[C]_o$ represent the concentration (ppm) of the substrate in solution time zero and time t of illumination, respectively, and k represent the apparent rate constant (min^{-1}). The findings are represented in Figure 10, and the apparent rate constants are summarized in Table 4. The results show that the reaction followed first-order kinetics with respect to CO and the rate constants were ranged from 134×10^{-4} to $469 \times 10^{-4}\,\mathrm{min}^{-1}$ by using loading from 33.3 mol% NiO/SnO_2 catalyst range from 0.1 to 0.35 gm, respectively.

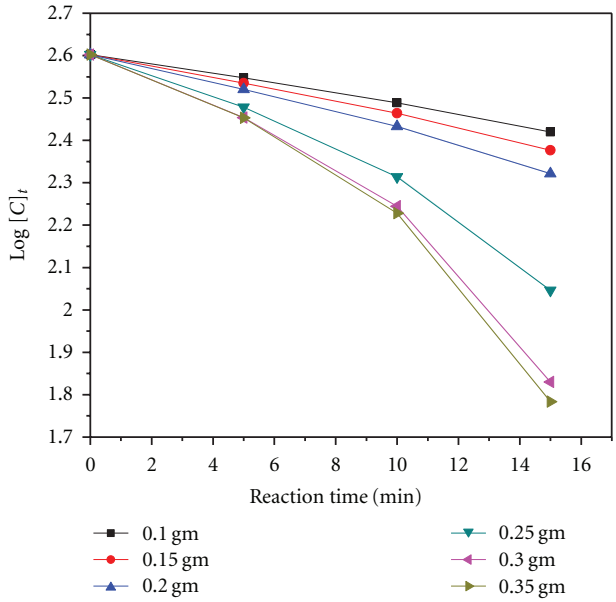

Figure 10

Table 4: Apparent rate constant (k) at different loading of 33.3 mol% NiO/SnO_2.

Loading of 33.3 mol% NiO/SnO_2, gm.	k, $min^{-1} \times 10^{-4}$
0.1	134
0.15	161
0.20	196
0.25	354
0.30	494
0.35	469

The first-order rate equation for CO given by:

$$R = k[\mathrm{CO}]. \quad (4)$$

4. Conclusions

The NiO/SnO_2 nanocomposites have been prepared by the simple coprecipitation method and further characterized by the XRD, SEM, TEM, UV-vis, and BET. The XRD patterns show that the prepared samples are rutile in structure with ≤5 nm in size. No impurity phase has been observed in XRD. The crystallanity, particle size, and lattice constant are decreasing with the increase in nickel concentration. The band gap of the doped samples show a narrowing effect as measured from the Tauc relation. The intensity of visible emission increases as the dopant concentration increases. Thus, the nickel doping can be used as a method to control the band gap and visible luminescence of the SnO_2 nanoparticles. The morphology of NiO/SnO_2 nanocomposites is spherical, and the distribution of the particle size is uniform as seen from EDX and TEM. The NiO/SnO_2 nanocomposites exhibits relatively high activity for photocatalytic oxidation of CO. Effects of NiO content and photocatalyst loading have been studied in detail. The reaction order with respect to CO was determined, The results show that the reaction followed first-order kinetics with respect to CO, and the rate constants were ranged from 134×10^{-4} to 469×10^{-4} min^{-1} by using loading from 33.3 mol% NiO/SnO_2 catalyst range from 0.1 to 0.35 gm, respectively. Due to simple preparation, high photocatalytic oxidation of CO and low cost, the NiO/SnO_2 photocatalyst will find wide application in the coming future of photocatalytic removal of pollutants.

Acknowledgments

The authors acknowledge with pleasure the financial support of this Project no. (210-247/431) by the Deanship of Scientific Research. They also acknowledge with pleasure the Deanship of Scientific Research, King Abdul-Aziz University, for the continuous guidance and support during the period of the project. They acknowledge deeply with pleasure all the partners that helped and encouraged this work at the Department of Chemistry, Faculty of Science and Department of Science, Faculty of Education at King Abdul-Aziz University.

References

[1] K. Gurunathan, P. Maruthamuthu, and M. V. C. Sastri, "Photocatalytic hydrogen production by dye-sensitized Pt/SnO_2 and $Pt/SnO_2/RuO_2$ in aqueous methyl viologen solution," *International Journal of Hydrogen Energy*, vol. 22, no. 1, pp. 57–62, 1997.

[2] W. W. So, K. J. Kim, and S. J. Moon, "Photo-production of hydrogen over the CdS-TiO_2 nano-composite particulate films treated with TiCl4," *International Journal of Hydrogen Energy*, vol. 29, no. 3, pp. 229–234, 2004.

[3] X. D. Yu, Q. Y. Wu, S. C. Jiang, and Y. H. Guo, "Nanoscale ZnS/TiO2 composites: preparation, characterization, and visible-light photocatalytic activity," *Materials Characterization*, vol. 57, no. 4-5, pp. 333–341, 2006.

[4] P. E. Jongh, D. De Vanmaekelbergh, and J. J. Kelly, "Cu2O: a catalyst for the photochemical decomposition of water?" *Chemical Communications*, no. 12, pp. 1069–1070, 1999.

[5] R. M. Mohamed and I. A. Mkhalid, "Characterization and catalytic properties of nano-sized Ag metal catalyst on TiO_2—SiO_2 synthesized by photo-assisted deposition and impregnation methods," *Journal of Alloys and Compounds*, vol. 501, no. 2, pp. 301–306, 2010.

[6] R. M. Mohamed and I. A. Mkhalid, "The effect of rare earth dopants on the structure, surface texture and photocatalytic properties of TiO2—SiO2 prepared by sol—gel method," *Journal of Alloys and Compounds*, vol. 501, no. 1, pp. 143–147, 2010.

[7] V. Keller and F. Garin, "Photocatalytic behavior of a new composite and oxides ternary system: WO3/SiCeTiO2 effect of the coupling of semiconductors in photocatalytic oxidation of methylethylketone in the gas phase," *Catalysis Communications*, vol. 4, pp. 377–383, 2003.

[8] J. H. Yan, Y. R. Zhu, Y. G. Tang, and S. Q. Zheng, "Nitrogen-dopedSrTiO3/TiO2 compositephotocatalysts for hydrogen-productionunder visible light irradiation," *Journal of Alloys and Compounds*, vol. 472, no. 1-2, pp. 429–433, 2009.

[9] R. Sasikala, A. Shirole, V. Sudarsan et al., "Highly dispersed phase of SnO2 on TiO2 nanoparticles synthesized by polyol-mediated route: photocatalytic activity for hydrogen generation," *International Journal of Hydrogen Energy*, vol. 34, no. 9, pp. 3621–3630, 2009.

[10] M. Stodolny and M. Laniecki, "Synthesis and characterization of mesoporous Ta2O5-TiO2 photocatalysts for water splitting," *Catalysis Today*, vol. 142, no. 3-4, pp. 314–319, 2009.

[11] T. Miwa, S. Kaneco, H. Katsumata et al., "Photocatalytic hydrogen production from aqueous methanol solution with $CuO/Al_2O_3/TiO_2$ nanocomposite," *International Journal of Hydrogen Energy*, vol. 35, no. 13, pp. 6554–6560, 2010.

[12] X. H. Zhou, Q. X. Cao, H. Huang, P. Yang, and Y. Hu, "Study on sensing mechanism of $CuO\text{-}SnO_2$ gas sensors," *Materials Science and Engineering B*, vol. 99, no. 1–3, pp. 44–47, 2003.

[13] T. Pagnier, M. Boulova, A. Galerie, A. Gaskov, and G. Lucazeau, "Reactivity of SnO_2-CuO nanocrystalline materials with H2S: a coupled electrical and Raman spectroscopic study," *Sensors and Actuators, B*, vol. 71, no. 1-2, pp. 134–139, 2000.

[14] I. S. Hwang, J. K. Choi, S. J. Kim et al., "Enhanced H2S sensing characteristics of SnO2 nanowires functionalized with CuO," *Sensors and Actuators, B*, vol. 142, no. 1, pp. 105–110, 2009.

[15] C. Li, W. Wei, S. Fang et al., "A novel CuO-nanotube/SnO_2 composite as the anode material for lithium ion batteries," *Journal of Power Sources*, vol. 195, no. 9, pp. 2939–2944, 2010.

[16] A. L. Patterson, "The Scherrer formula for x-ray particle size determination," *Physical Review Online Archive*, vol. 56, pp. 978–982, 1939.

[17] J. H. Yu and G. M. Choi, "Electrical and CO gas sensing properties of ZnO—SnO2 composites," *Sensors and Actuators, B*, vol. 52, no. 3, pp. 251–256, 1998.

[18] L. M. Fang, X. T. Zu, Z. J. Li et al., "Microstructure and luminescence properties of Co-doped SnO_2 nanoparticles synthesized by hydrothermal method," *Journal of Materials Science*, vol. 19, no. 8-9, pp. 868–874, 2008.

[19] T. Takagahara and K. Takeda, "Theory of the quantum confinement effect on excitons in quantum dots of indirect-gap materials," *Physical Review B*, vol. 46, no. 23, pp. 15578–15581, 1992.

[20] L. Chun-Ming, F. Li-Mei, Z. Xiao-Tao, and Z. Wei-Lie, "The influence of nickel dopant on the microstructure and optical properties of SnO2 nano-powders," *Chinese Physics*, vol. 16, no. 1, pp. 95–99, 2007.

[21] A. E. Rakhshani, Y. Makdisi, and H. A. Ramazaniyan, "Electronic and optical properties of fluorine-doped tin oxide films," *Journal of Applied Physics*, vol. 83, no. 2, pp. 1049–1057, 1998.

[22] Y. R. Park and K. J. Kim, "Sputtering growth and optical properties of [100]-oriented tetragonal SnO2 and its Mn alloy films," *Journal of Applied Physics*, vol. 94, no. 10, pp. 6401–6404, 2003.

[23] N. Barreau, J. C. Bernede, S. Marsillac, and A. Mokrani, "Study of low temperature elaborated tailored optical band gap [beta]-In2S3-3xO3x thin films," *Journal of Crystal Growth*, vol. 235, no. 1–4, pp. 439–449, 2002.

[24] B. Sasi, K. G. Gopchandran, P. K. Manoj, P. Koshy, P. P. Rao, and V. K. Vaidyan, "Preparation of transparent and semiconducting NiO films," *Vacuum*, vol. 68, no. 2, pp. 149–154, 2002.

[25] Z. L. Jin, X. L. Zhang, Y. X. Li, S. B. Li, and G. X. Lu, "5.1% apparent quantum efficiency for stable hydrogen generation over eosin-sensitized CuO/TiO_2 photocatalyst under visible light irradiation," *Catalysis Communications*, vol. 8, no. 8, pp. 1267–1273, 2007.

[26] S. P. Xu and D. D. Sun, "Significant improvement of photocatalytic hydrogen generation rate over TiO_2 with deposited CuO," *International Journal of Hydrogen Energy*, vol. 34, no. 15, pp. 6096–6104, 2009.

[27] A. A. Nada, M. H. Barakat, H. A. Hamed, N. R. Mohamed, and T. N. Veziroglu, "Studies on the photocatalytic hydrogen production using suspended modified TiO2 photocatalysts," *International Journal of Hydrogen Energy*, vol. 30, no. 7, pp. 687–691, 2005.

[28] N. L. Wu and M. S. Lee, "Enhanced TiO_2 photocatalysis by Cu in hydrogen production from aqueous methanol solution," *International Journal of Hydrogen Energy*, vol. 29, no. 15, pp. 1601–1605, 2004.

[29] X. J. Zheng, L. F. Wei, Z. H. Zhang et al., "Research on photocatalytic H2 production from acetic acid solution by Pt/TiO_2 nanoparticles under UV irradiation," *International Journal of Hydrogen Energy*, vol. 34, no. 22, pp. 9033–9041, 2009.

[30] X. L. Fu, J. L. Long, X. X. Wang et al., "Photocatalytic reforming of biomass: a systematic study of hydrogen evolution from glucose solution," *International Journal of Hydrogen Energy*, vol. 33, no. 22, pp. 6484–6491, 2008.